frontiers in Built Environment

ORIGINAL RESEARCH
published: 22 June 2015
doi: 10.3389/fbuil.2015.00008

The 2015 Gorkha Nepal earthquake: insights from earthquake damage survey

Katsuichiro Goda[1], Takashi Kiyota[2], Rama Mohan Pokhrel[2], Gabriele Chiaro[2], Toshihiko Katagiri[2], Keshab Sharma[3] and Sean Wilkinson[4]*

[1] Department of Civil Engineering, University of Bristol, Bristol, UK, [2] Institute of Industrial Science, University of Tokyo, Tokyo, Japan, [3] Department of Civil and Environmental Engineering, University of Alberta, Edmonton, AB, Canada, [4] School of Civil Engineering and Geosciences, Newcastle University, Newcastle upon Tyne, UK

The 2015 Gorkha Nepal earthquake caused tremendous damage and loss. To gain valuable lessons from this tragic event, an earthquake damage investigation team was dispatched to Nepal from 1 May 2015 to 7 May 2015. A unique aspect of the earthquake damage investigation is that first-hand earthquake damage data were obtained 6–11 days after the mainshock. To gain deeper understanding of the observed earthquake damage in Nepal, the paper reviews the seismotectonic setting and regional seismicity in Nepal and analyzes available aftershock data and ground motion data. The earthquake damage observations indicate that the majority of the damaged buildings were stone/brick masonry structures with no seismic detailing, whereas the most of RC buildings were undamaged. This indicates that adequate structural design is the key to reduce the earthquake risk in Nepal. To share the gathered damage data widely, the collected damage data (geo-tagged photos and observation comments) are organized using Google Earth and the kmz file is made publicly available.

Keywords: 2015 Nepal earthquake, earthquake damage survey, building damage, ground motion, aftershocks

OPEN ACCESS

Edited by:
Solomon Tesfamariam, The University of British Columbia, Canada

Reviewed by:
Vladimir Sokolov, Karlsruhe Institute of Technology, Germany
Takeshi Koike, Kyoto University, Japan

****Correspondence:***
Katsuichiro Goda, Department of Civil Engineering, University of Bristol, Queen's Building, University Walk, Bristol BS8 1TR, UK
katsu.goda@bristol.ac.uk

Specialty section:
This article was submitted to Earthquake Engineering, a section of the journal Frontiers in Built Environment

Received: *28 May 2015*
Accepted: *08 June 2015*
Published: *22 June 2015*

Citation:
Goda K, Kiyota T, Pokhrel RM, Chiaro G, Katagiri T, Sharma K and Wilkinson S (2015) The 2015 Gorkha Nepal earthquake: insights from earthquake damage survey. Front. Built Environ. 1:8. doi: 10.3389/fbuil.2015.00008

Introduction

An intense ground shaking struck Central Nepal on 25 April 2015 (local time 11:56 a.m.). The moment magnitude of the earthquake was M_w7.8 with its hypocenter located in the Gorkha region (about 80 km north–west of Kathmandu). The earthquake occurred at the subduction interface along the Himalayan arc between the Indian plate and the Eurasian plate (Avouac, 2003; Ader et al., 2012). The earthquake rupture propagated from west to east and from deep to shallow parts of the shallowly dipping fault plane [United States Geological Survey (USGS), (2015)], and consequently, strong shaking was experienced in Kathmandu and the surrounding municipalities. This was the largest event since 1934, M_w8.1 Bihar–Nepal earthquake (Ambraseys and Douglas, 2004; Bilham, 2004). The 2015 mainshock destroyed a large number of buildings and infrastructure in urban and rural areas, and triggered numerous landslides and rock/boulder falls in the mountain areas, blocking roads, and hampering rescue and recovery activities. Moreover, aftershock occurrence has been active since the mainshock; several major aftershocks (e.g., M_w6.7 and M_w7.3 earthquakes in the Kodari region, north–east of Kathmandu) caused additional damage to rural towns and villages in the northern part of Central Nepal. As of 26 May 2015, the earthquake damage statistics for Nepal from the 25 April 2015 mainshock stand at the total

number of 8,510 deaths and 199 missing[1]. In addition, the major aftershock that occurred on 12 May 2015 caused 163 deaths/missing. Center for Disaster Management and Risk Reduction Technology (CEDIM), (2015) reports that the total economic loss is in the order of 10 billion U.S. dollars, which is about a half of Nepal's gross domestic product. The 2015 earthquakes will have grave long-term socioeconomic impact on people and communities in Nepal [United Nations Office for the Coordination of Humanitarian Affairs (UN-OCHA), (2015)].

Earthquake field observations provide raw damage data of existing built environments and are useful for developing empirical correlation between ground motion intensity and damage severity for earthquake impact assessment of future events. To gain valuable lessons from this tragic event, an earthquake damage investigation team was jointly organized by the Japan Society of Civil Engineers and the Japan Geotechnical Society, and was dispatched to Nepal from 1 May 2015 to 7 May 2015. The survey trip was planned in such away that relatively large geographical areas that were affected by the earthquakes were covered to grasp spatial features of the damage in the earthquake-hit regions. A unique aspect of this damage investigation is that the data were collected at the early stage of disaster response and recovery (6–11 days after the mainshock), and thus first-hand earthquake damage observations were obtained before major repair work. The collected damage data, in the form of geo-tagged photos and some measurements (e.g., size of a landslide), are useful for other earthquake damage reconnaissance teams who visit Nepal several weeks after the mainshock, and serve as a starting point of longitudinal research of a recovery process from the earthquakes. To achieve this goal, damage photos that were taken during the survey trip are organized using Google Earth and are made publicly available; the kmz file is provided as supplementary resource of this paper. Viewers can download the photos directly and can use them for research and educational purposes; all photos are geo-tagged and are accompanied by brief comments.

This paper summarizes key findings of ground shaking damage in Nepal, and is organized as follows. To link building damage observations with available seismological data, seismotectonic setting of Nepal is reviewed, and earthquake rupture process and aftershock data, which are available from the U.S. Geological Survey (USGS), are analyzed to gain scientific insights into ground motions that were experienced during the mainshock and major aftershocks. It is important to note that strong motion observation networks in Nepal are not well developed and data are not publicly accessible. This means that the estimation of observed ground motions at building damage sites is highly uncertain. Currently, recorded time-history data of strong motion are only available at the KATNP station, which is located in the city center of Kathmandu. In this study, strong motion data at KATNP are analyzed and the results, in the form of elastic response spectra, are discussed by comparing with relevant ground motion prediction models [e.g., Kanno et al. (2006) and Boore and Atkinson (2008)] and with well-recorded strong motion data from the 2008 M_w7.9 Wenchuan China earthquake (Lu et al., 2010), seismological features of which are broadly similar to the 2015 Nepal earthquake. Furthermore, issues related to ground motion estimation for prompt earthquake impact assessment [e.g., Jaiswal and Wald (2010) and Center for Disaster Management and Risk Reduction Technology (CEDIM), (2015)] are discussed by examining how the way source-to-site distance measures, as in ground motion prediction equations, are evaluated affects the scenario shake map of a large subduction event within a fault rupture zone (note: size of the fault rupture zone can be in the order of a few hundred kilometers for M_w8.0+ earthquakes). Such investigations provide new insights for improvements in producing more reliable scenario shake maps and prompt earthquake impact assessments (Goda and Atkinson, 2014). Subsequently, building typology in Nepal is reviewed briefly, followed by earthquake damage observations in Kathmandu, Melamchi, Trishuli, and Baluwa. Finally, key lessons from the 2015 Nepal earthquake are summarized.

Regional Seismicity and Ground Motion

This section aims at providing with relevant seismological information for interpreting earthquake damage survey observations in Nepal (which are discussed in the following section). First, seismotectonic and seismological aspects of the on-going mainshock–aftershock sequence are reviewed by analyzing available earthquake catalog data and source rupture models of the mainshock. Strong ground motion recordings at KATNP are analyzed to estimate the observed ground motion intensity in Kathmandu. Subsequently, scenario shake maps are generated by considering different source-to-site distance measures to highlight the influence of finite-fault source representation for a large earthquake in applications to prompt earthquake impact assessment.

Seismotectonic Setting and Seismic Hazard in Nepal

Nepal is located along the active Main Himalayan Thrust arc, where the subducting Indian plate and the overriding Eurasian plate interact. This region accommodates approximately a half of the tectonic convergence between these two plates, i.e., about 20 mm/year (Avouac, 2003; Ader et al., 2012). The locked part of the subduction interface has a low-dip angle (about 10°) and is located at depths of 4–18 km (Bilham, 2004), and has potential to generate M_w8+ earthquakes (Gupta, 2006).

Historically, Nepal hosted several large earthquakes (Ambraseys and Douglas, 2004; Bilham, 2004). A map of Nepal and locations of major historical seismic events are shown in **Figure 1**. Western Nepal experienced a M_w8.2 event in 1505. This event occurred west of the rupture zone of the 2015 earthquake and accumulated strain in this seismic gap region has not been released since then; thus, there is high potential for future large earthquakes in the western region. In Eastern Nepal, two known major earthquakes occurred in 1833 and 1934. In particular, the 1934 M_w8.1 Bihar–Nepal earthquake was destructive and caused many fatalities (+10,000 deaths). The 2015 Gorkha–Kodari earthquakes have ruptured a fault section that overlaps with the fault rupture plane of the 1934 earthquake (see **Figure 1**). It is noted that the rupture planes of

[1]http://earthquake-report.com/

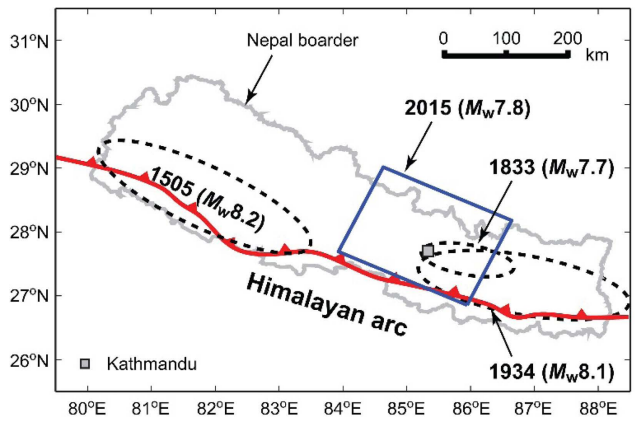

FIGURE 1 | Major historical earthquakes in Nepal along the Himalayan arc. The locations of three historical earthquakes (1505, 1833, and 1934) are approximate. For the M_w7.8 mainshock, the fault plane model by the USGS is shown.

the 1934 and 2015 earthquakes are directly beneath Kathmandu, although the locations of their hypocenters are east and west of Kathmandu, respectively.

Recently, several probabilistic seismic hazard studies have been conducted for Nepal by employing updated seismic source zone models based on improved earthquake catalogs and modern ground motion models [e.g., Nath and Thingbaijam (2012) and Ram and Wang (2013)]. The estimated peak ground acceleration (PGA) with 10% probability of exceedance in 50 years (i.e., return period of 475 years) in Western Nepal ranges between 0.5and 0.6 g, whereas that in Eastern Nepal ranges between 0.3 and 0.6 g. These hazard estimates are obtained for rock sites, therefore, when typical soil sites are considered (e.g., Kathmandu Valley), they need to be increased. An important observation is that the ground motion shaking in Kathmandu during the 2015 mainshock (which is discussed in detail in the following) was less than the PGA estimates with 10% probability of exceedance in 50 years, which may be considered as a basis for seismic design in Nepal.

Fault Rupture Model of the 25 April 2015 Mainshock

Several earthquake rupture models for the 2015 mainshock have been developed [e.g., United States Geological Survey (USGS) (2015); Yagi (2015)]. A common feature of the estimated slip distributions is that large slips occurred north and north–east of Kathmandu, and the rupture propagated from the hypocenter (north–west of Kathmandu) toward east as well as south (deeper to shallower depth). The slip distribution of the USGS model is illustrated in **Figure 2A**. The fault length and width of the rupture plane are 220 and 165 km, respectively, and its strike and dip are 295° and 10°, respectively. **Figure 3** overlays the route of the survey trip over the USGS source model to put visited locations (i.e., Melamchi, Trishuli, and Baluwa) into perspective with respect to the earthquake slip distribution. The USGS source model has its maximum slip of 3.11 m (north of Kathmandu). It is also interesting to observe that the estimated slip near the hypocenter is 1.29 m, which is about 40% of the maximum slip, and its distance from the maximum slip sub-fault (i.e., asperity) is about 70 km. By analyzing numerous earthquake rupture models statistically, Mai et al. (2005) found that the rupture often nucleates in the regions of low-to-moderate slip (sub-faults with slip <2/3 of the maximum slip) and close to the maximum slip sub-fault. The rupture nucleation of the 2015 mainshock (i.e., slip and location at the hypocenter) is in good agreement with these empirical rules suggested by Mai et al. (2005).

Aftershocks

In post-earthquake situations, one of the major concerns for evacuees and emergency response teams is the occurrence of major aftershocks, triggering secondary hazards. Generally, a larger earthquake is followed by more aftershocks, and returning to a background level of seismic activities takes longer. **Figure 2A** shows the spatial distribution of aftershocks that occurred before 25 May 2015 (30 days since the mainshock). The aftershock data are obtained from the USGS NEIC catalog[2]. Immediately after the mainshock, a moderate (M_w6.6) aftershock occurred near the hypocenter. On the other hand, the majority of aftershocks occurred in the Kodari region (north–east of Kathmandu); a notable event was the 12 May 2015 M_w7.3 aftershock, which caused additional damage and casualties. Comparison of the aftershock distribution with respect to the slip distribution of the mainshock indicates that the major aftershocks do not occur very near to the mainshock asperity (with large slip) but they occur in the surrounding areas of the mainshock asperity. This is because the spatial and temporal characteristics of aftershocks are the manifestation of internal crustal dynamics involving the redistribution of stress and displacement fields (Stern, 2002; Heuret et al., 2011).

To gain further insights into the aftershock occurrence process of the 2015 mainshock–aftershock sequence, statistical analysis of aftershock data is carried out by applying the Gutenberg–Richter law and the modified Omori law (Shcherbakov et al., 2005); the completeness magnitude is set to 4.5 for the analyses. The Gutenberg–Richter law describes the frequency–magnitude characteristics of an aftershock sequence, whereas the modified Omori law models a temporal decay of an aftershock occurrence rate. The fitting of the 2015 Nepal aftershock data to the Gutenberg–Richter relationship is satisfactory (**Figure 2B**); the estimated slope parameter (i.e., *b*-value) is −0.862. This slope is slightly gentler (i.e., more productive for larger aftershocks) than the typical *b*-value for global subduction earthquakes but within the expected range (Shcherbakov et al., 2013). **Figure 2C** shows that the modified Omori's law fits well with the aftershock data. The obtained parameters are typical for global subduction earthquakes (Shcherbakov et al., 2013). For example, the temporal decay parameter (i.e., *p* value, power parameter in the equation shown in **Figure 2C**) is 1.049, which is close to the global average of about 1.2 (by taking into account inherent variability of this parameter). The above results support the applicability of well-established empirical laws for characterizing the 2015 Nepal aftershock data. This is a useful confirmation from seismic risk management viewpoints because initial estimates of aftershock-related hazard can be obtained from

[2]http://earthquake.usgs.gov/earthquakes/search/

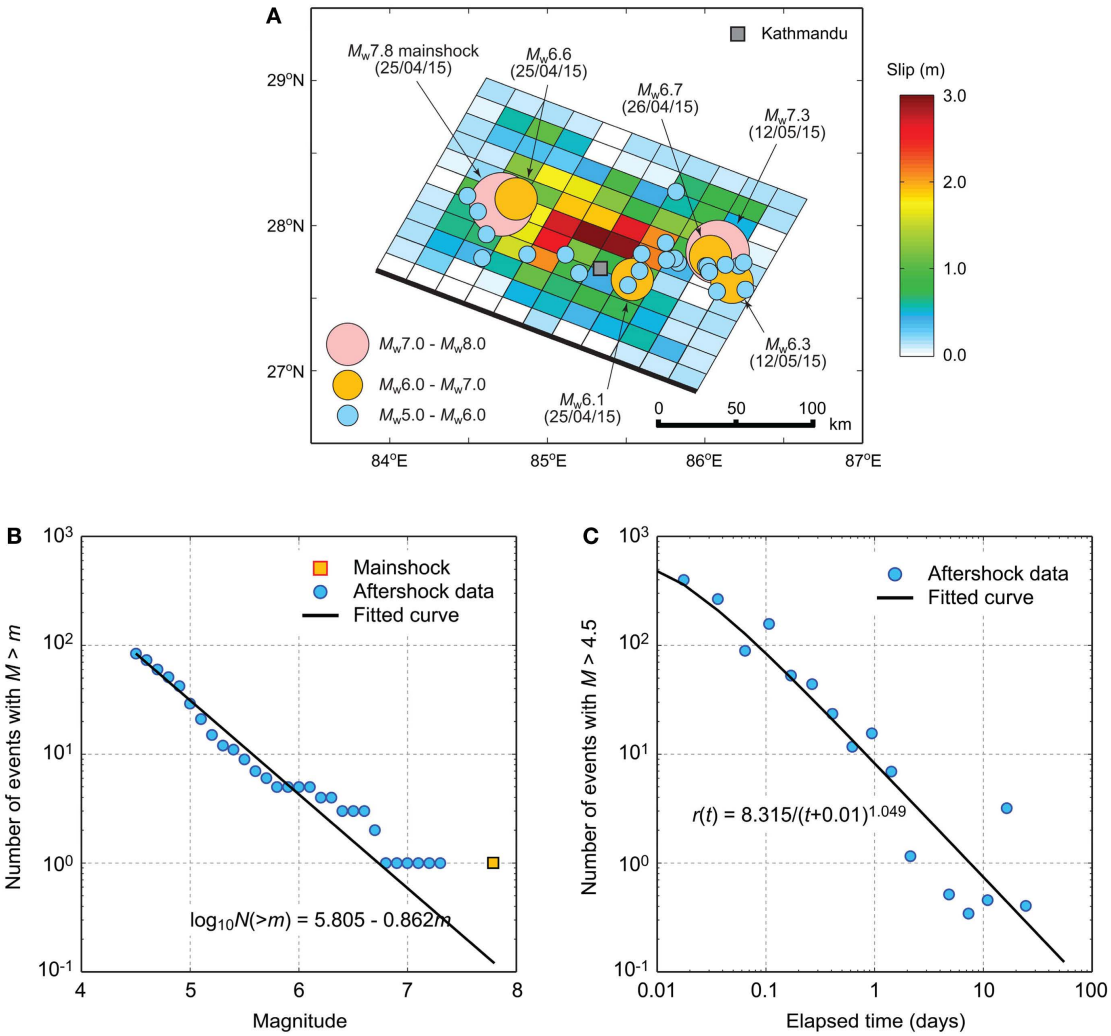

FIGURE 2 | **(A)** Aftershock distribution of the 2015 earthquake sequence; an earthquake source model by the USGS is shown. **(B)** Gutenberg–Richter relationship of the 2015 earthquake sequence. **(C)** Modified Omori law of the 2015 earthquake sequence.

the empirical aftershock models immediately after the mainshock (before real-time data are collected and analyzed).

Ground Motion in Kathmandu

The accelerograms recorded at KATNP are publicly available[3]. In light of poor strong motion network in Nepal, the recorded ground motion data at KATNP are invaluable and serve as a benchmark in estimating ground motion intensity at unobserved locations in Kathmandu. **Figure 4** shows the location of the KATNP station; the map also shows the locations of the earthquake damage survey sites in Kathmandu. The KATNP station is located near the historical district in the city center (e.g., Durbar Square), where severe damage and collapse of old historical buildings occurred.

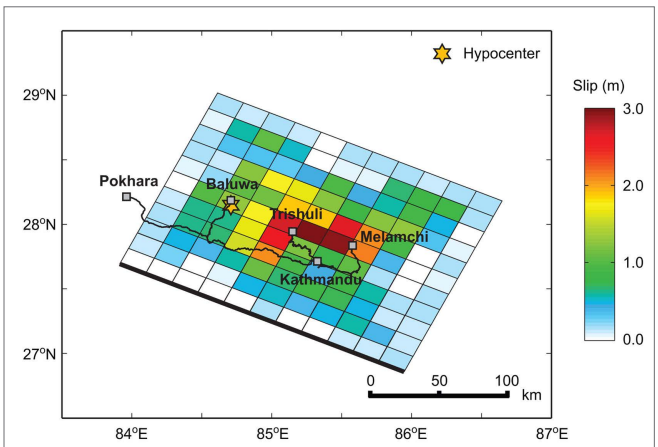

FIGURE 3 | **Earthquake damage survey locations**.

[3]http://www.strongmotioncenter.org/

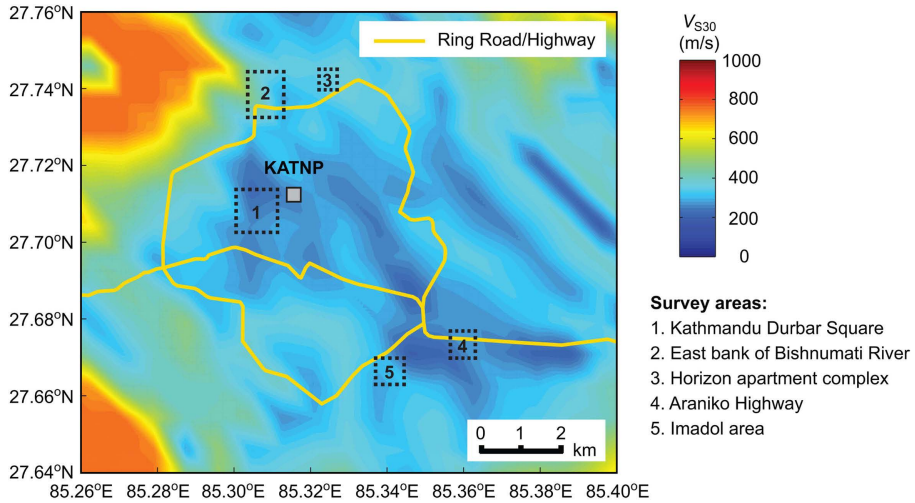

FIGURE 4 | **Location of the strong motion recording station KATNP and earthquake damage survey locations in Kathmandu**.

Prior to ground motion data analysis and estimation, it is important to review typical site conditions in Kathmandu, as they affect ground motion intensity significantly. Kathmandu is located in the Kathmandu Basin, where thick lacustrine and fluvio-lacustrine sediments are deposited (Sakai et al., 2002). The thickness of sediments (i.e., depth to bedrock) is in the range of 550–650 m. The setting of the Kathmandu Valley is similar to Mexico City (Paudyal et al., 2012), noting that during the 1985 Michoacán earthquake, long-period ground motions were significantly amplified in Mexico City due to soft lakebed deposits and caused catastrophic damage to mid-to-high-rise buildings. A seismic microzonation study in Kathmandu, conducted by Paudyal et al. (2012), indicates that the dominant periods of the ground at sites inside the Ring Road (see **Figure 4**) are between 1.0 and 2.0 s (i.e., high potential for resonating with long-period ground motions), and that the dominant period is correlated with the thickness of Pliocene and Quaternary deposits. The KATNP station is located within the long-dominant-period zone.

Another useful source of information in assessing site amplification potential of near-surface soil deposits in Kathmandu is the USGS global V_{S30} server (Wald and Allen, 2007)[4]. V_{S30} is the average shear-wave velocity in the uppermost 30 m and is often employed as a proxy site parameter in ground motion models [e.g., Kanno et al. (2006) and Boore and Atkinson (2008)]. Wald and Allen (2007) correlated V_{S30} data with topographic slope to derive the first-order estimate of the site amplification for two tectonic regimes, active and stable continental regions. The database is implemented to develop USGS ShakeMaps (Wald et al., 2005)[5], which are used for rapid earthquake impact assessment (Jaiswal and Wald, 2010)[6]. **Figure 4** shows the V_{S30} contour map in Kathmandu. The map indicates that the central part of Kathmandu has soft surface deposits (typically NEHRP site class D, V_{S30} between 180 and 360 m/s). The V_{S30} value at the KATNP station is 250 m/s. It is noteworthy that V_{S30} is applicable to near-surface site amplification only; amplification of long-period seismic waves due to a large-scale geological structure (e.g., basin) should be taken into account separately.

Figures 5A,B show recorded accelerograms (three components) at KATNP for the M_w7.8 mainshock and for the M_w7.3 aftershock, respectively (note: among other recorded aftershock ground motions at KATNP, the M_w7.3 aftershock records show the most significant effects). An inspection of the time-history data indicates that the PGA of the recorded ground motions is about 150–170 and 70–80 cm/s^2 for the M_w7.8 mainshock and the M_w7.3 aftershock, respectively. These are significantly smaller than the PGA estimates with 10% probability of exceedance in 50 years from the recent regional seismic hazard studies (Nath and Thingbaijam, 2012; Ram and Wang, 2013). It is also observed that long-period components are present in the M_w7.8 mainshock records (**Figure 5A**). To further investigate the extent of ground shaking at KATNP, 5%-damped response spectra of the recorded accelerograms for the M_w7.8 mainshock and the M_w7.3 aftershock are calculated and compared in **Figure 5C**. The results suggest that the amplitudes of response spectra for the mainshock are greater than those for the major aftershock (also applicable to other aftershocks). For the M_w7.8 mainshock, two large peaks of response spectra are present at vibration periods around 0.2–0.6 s (N–S component only) and around 4.0–6.0 s (both N–S and E–W components). The former is attributed to direct shaking due to near-source ruptures, whereas the latter is caused by the combination of rich long-period content of seismic waves at source (because of large moment magnitude) and site amplification due to the basin effects. Given the existing building stock in Kathmandu/Nepal (the majority of buildings are low-to-mid rise and thus are likely to have vibration periods <1.0 s; Chaulagain et al., 2015), the main causes of severe structural damage and collapse of buildings in

[4]http://earthquake.usgs.gov/hazards/apps/vs30/
[5]http://earthquake.usgs.gov/earthquakes/shakemap/
[6]http://earthquake.usgs.gov/earthquakes/pager/

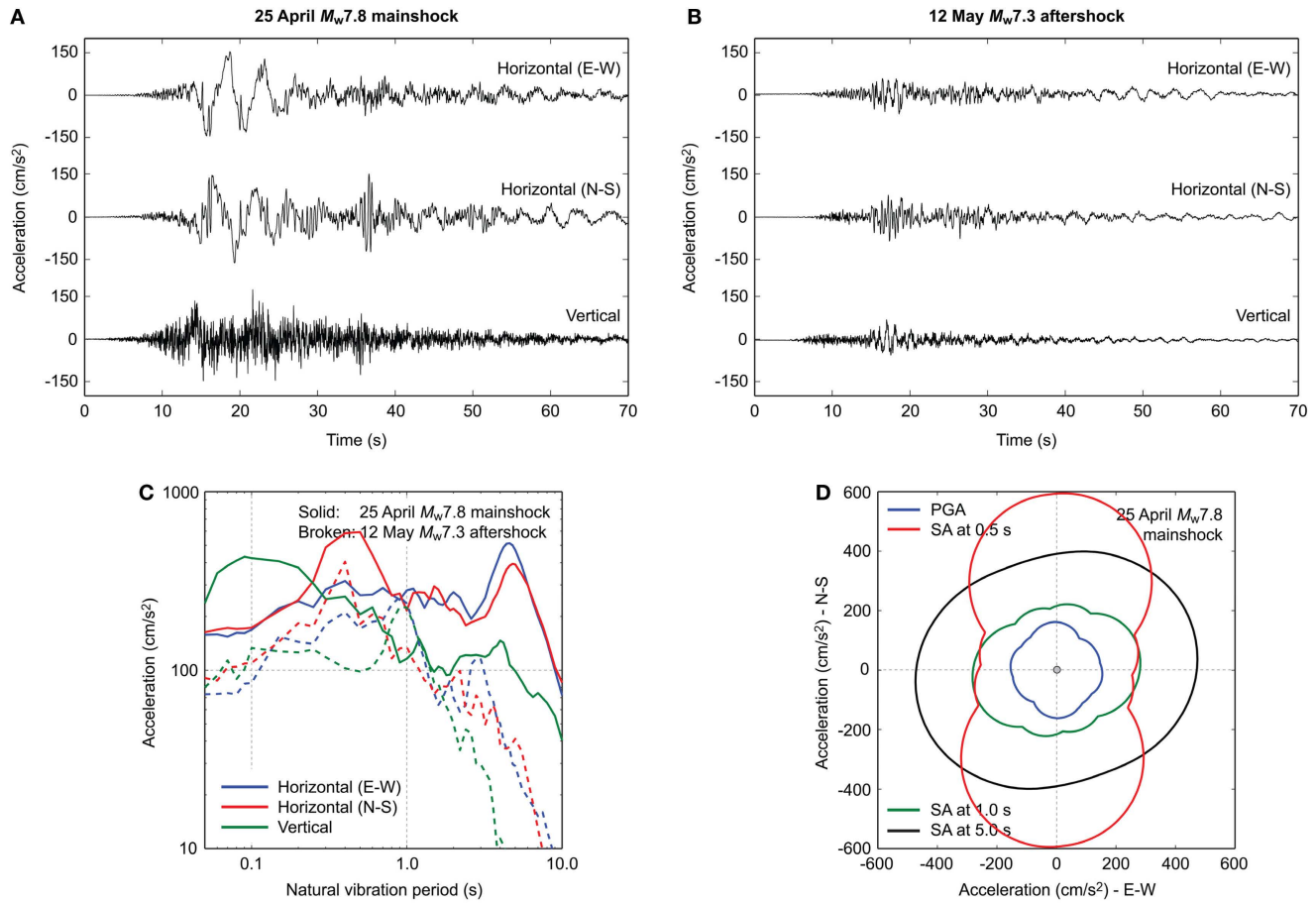

FIGURE 5 | **(A)** Recorded accelerograms at KATNP for the M_w7.8 mainshock. **(B)** Recorded accelerograms at KATNP for the M_w7.3 aftershock. **(C)** 5%-damped spectral accelerations (SA) of the recorded accelerograms at KATNP for the M_w7.8 mainshock and the M_w7.3 aftershock. **(D)** Polar plots of the PGA and spectral accelerations at 0.5, 1.0, and 5.0 s of the rotated accelerograms at KATNP for the M_w7.8 mainshock.

Kathmandu are due to the large peak in the short vibration period range. It is important to point out that buildings in Kathmandu were largely unaffected by the long-period ground motions in the Kathmandu Valley because of non-resonance. This was fortunate in the context of the current disaster. However, earthquake engineers should pay careful attention to long-period ground motions (Takewaki et al., 2011), when tall buildings are constructed in the central part of the Kathmandu Valley.

To further examine the orientation of ground motion parameters at KATNP for the M_w7.8 mainshock, PGA and 5%-damped spectral accelerations are computed by rotating accelerograms recorded at KATNP from 0° to 360° (Hong and Goda, 2007). The polar plots of PGA and spectral accelerations at 0.5, 1.0, and 5.0 s are shown in **Figure 5D**. The results are useful for understanding the orientation dependency of the peak seismic demand in the near-fault region (Huang et al., 2008). The results indicate that the spectral acceleration at 0.5 s (i.e., large response spectral peak in the short-vibration period range) is highly polarized; the ratio of the maximum-to-minimum response is about 2.5, while the degree of such polarization of the response spectra is much less pronounced at other vibration periods. Although it is beyond the scope of this study, a further insight can be gained by investigating the effects of the orientation of ground motion with regard to the structural axis of damaged versus non-damaged buildings near the KATNP station.

Comparison of Observed Ground Motion in Kathmandu with Ground Motion from the 2008 Wenchuan Earthquake and Predicted Ground Motion

Due to the limited availability of recorded ground motions in Central Nepal, ground motion estimation may need to rely on: (1) ground motion data from other seismic regions having broad similarity with the target region [e.g., Sharma et al. (2009)], (2) empirical ground motion prediction models [e.g., Nath and Thingbaijam (2011)], or (3) ground motion simulations [e.g., Harbindu et al. (2014)]. In this study, the first two options are explored to gain insights into actual ground motions for the M_w7.8 mainshock.

For Option 1, ground motion data from the 2008 M_w7.9 Wenchuan earthquake (Lu et al., 2010) are analyzed. This

earthquake is chosen because seismotectonic settings in Nepal and Tibet (i.e., southern and eastern sides of the Tibetan Plateau) are broadly similar and their earthquake magnitudes are comparable. The Wenchuan earthquake occurred along the Longmenshan fault Sichuan, China. The amplitude–distance plots of PGA and spectral accelerations at 0.5and 5.0 s are shown in **Figure 6**; only records at soft soil sites (V_{S30} <400 m/s) are considered. The rupture distance (R_{rup}, shortest distance from a site of interest to the fault rupture plane) for the Wenchuan data is calculated using the fault plane model by Ji (2008).

For Option 2, a ground motion model by Kanno et al. (2006) (hereafter Kanno06) is adopted. This prediction equation was developed by using ground motion records from Japanese earthquakes and from worldwide shallow crustal earthquakes (i.e., Next Generation Attenuation database). The Kanno06 equation is selected among other applicable models [e.g., Boore and Atkinson (2008), Sharma et al. (2009), and Harbindu et al. (2014)] for three reasons. The first reason is that the performance test of various ground motion models conducted by Nath and Thingbaijam (2011) indicates that the Kanno06 equation is superior to other candidate models in predicting PGA at rock sites in Northern India and Nepal. Second, the applicable moment magnitude range of the Kanno06 equation covers the moment magnitude of the 2015 Nepal earthquake; for instance, regional equations by Sharma et al. (2009) and Harbindu et al. (2014) are not applicable to M_w8-class earthquakes. Third, the Kanno06 equation adopts R_{rup} as a representative distance measure, while the equation by Boore and Atkinson (2008) (hereafter BA08) adopts the Joyner–Boore distance (R_{jb}, shortest distance from a site of interest to the projected fault rupture plane on Earth's surface). The use of R_{jb} can be problematic because ground motion intensity for the locations above the fault rupture plane is evaluated using a uniform value of $R_{jb} = 0$ km (which results in significant bias of predicted ground motion intensity). This issue is revisited in the next subsection.

Figure 6 compares observed ground motions at KATNP (i.e., **Figure 5**) with the ground motion data from the M_w7.9 Wenchuan earthquake as well as the Kanno06 model. The rupture distance for KATNP (=11.1 km) is calculated using the USGS finite-fault plane model (i.e., **Figure 2A**). For the Kanno06 model, 16th and 84th percentile curves are also shown to indicate a typical range of predicted ground motion variability. **Figure 6A** indicates that the observed PGA at KATNP is significantly smaller than the Wenchuan data in the similar distance range and the predicted PGA based on the Kanno06 equation (below the 16th percentile curve). The below-average trend of the observed ground motion intensity, in comparison with the Wenchuan data and the Kanno06 model, persists for spectral accelerations at vibration periods <2.0 s (**Figure 6B**). These comparisons indicate that the level of short-period ground motion near KATNP during the 2015 mainshock was smaller than expected ground motion levels based on empirical data/models for similar scenarios. On the other hand, **Figure 6C** shows an opposite trend: the long-period spectral acceleration at KATNP is significantly greater than the counterparts based on the Wenchuan data and the Kanno06 model. The large spectral acceleration in the long vibration period range is attributed to the basin effects. It is also interesting to note that the recent ground motion prediction model, such as Boore et al. (2014), can take into account the basin effects using a depth-to-bedrock parameter [note: in **Figure 6**, the equation by Boore et al. (2014) is not considered because it is based on R_{jb}]. Using the empirical model by Boore et al. (2014), the expected site amplification due to the basin effects is a factor of two for vibration periods longer than 2.0 s; the observed long-period spectral acceleration can be better explained. Therefore, it is important to adopt advanced ground motion models that can account for major systematic components (e.g., faulting mechanism and basin amplification) in predicting ground motion intensity for future earthquakes.

Scenario Shake Map

Rapid earthquake impact reports [e.g., Center for Disaster Management and Risk Reduction Technology (CEDIM), (2015)] are useful because emergency officers and international aiding agencies can appreciate the expected level of destruction due to an earthquake at the very early stage of a disaster. In producing rapid earthquake impact assessment, scenario shake maps are the essential input. In these applications, shake maps are generated by using a suitable ground motion model together with observed

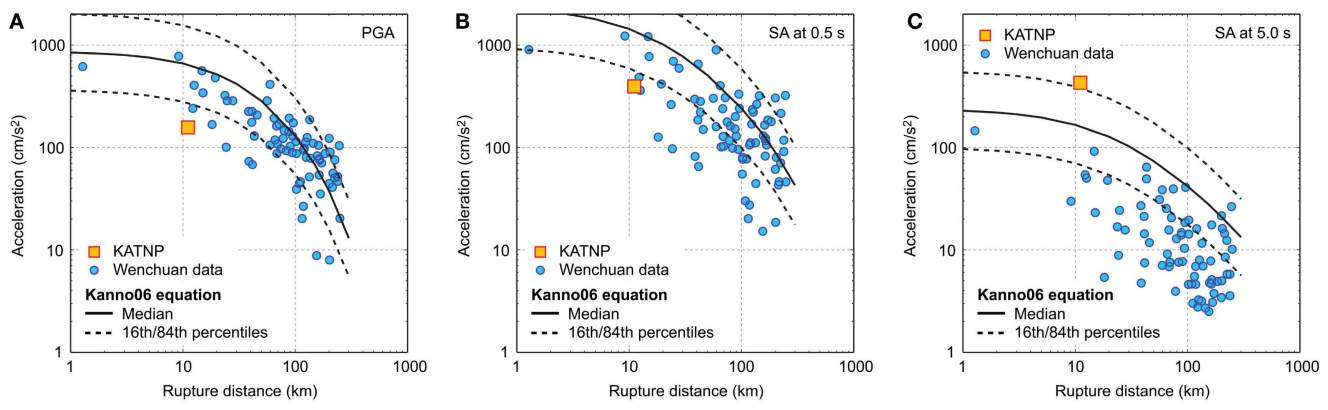

FIGURE 6 | Comparison of the observed PGA (A) and spectral accelerations [0.5 s in (B) and 5.0 s in (C)] at KATNP with the M_w7.9 Wenchuan ground motion data and with the ground motion model by Kanno et al. (2006).

instrumental data and seismic intensity information (e.g., DYFI; Atkinson and Wald, 2007)[7]. In seismic regions with limited monitoring capability of strong motion, shake maps are more dependent on the accuracy of an adopted ground motion model as well as on initial estimates of the seismic event (e.g., moment magnitude). This is because there will not be many real-time observations to constrain the shake map predictions.

Modern ground motion models adopt extended-source-based distance measures, such as R_{rup} and R_{jb} (i.e., calculation of these distance measures requires a fault plane model). A simpler representation of an earthquake source is a point source model; in this case, hypocentral and epicentral distances, R_{hypo} and R_{epi}, are often used. When a slip distribution is available, another useful distance measure is the shortest distance to the asperity R_{asp} (Goda and Atkinson, 2014). For large subduction events having large fault plane dimensions, the calculated distance measures can vary significantly, depending on how a fault plane model is defined and which distance measure is adopted. For instance, for the M_w7.8 mainshock, distance measures at KATNP are evaluated as: R_{rup} = 11.1 km, R_{jb} = 0.1 km (numerical lower bound), R_{hypo} = 85.3 km, R_{epi} = 76.8 km, and R_{asp} = 29.4 km. The influence of distance measures is particularly significant for large magnitude events.

The above-mentioned problem has an important implication on shake map generation for a large earthquake. To demonstrate this for the M_w7.8 mainshock, four scenario PGA shake maps are developed by considering different distance measures and ground motion models. The results are shown in **Figure 7**. **Figures 7–C** are based on the Kanno06 model together with R_{rup}, R_{hypo}, and R_{asp}, respectively, whereas **Figure 7D** is based on the BA08 model with R_{jb}. For all shake maps, V_{S30} information at individual sites is taken into account. Strictly, R_{hypo} and R_{asp} should not be used in the Kanno06 model (as the distance measures and the model development process are incompatible); this is for illustration only. **Figure 7A** shows the predicted PGAs at sites above the fault plane are large (0.5–0.7 g) and predicted PGA values gradually decrease toward north (i.e., the fault plane becomes deeper). **Figures 7B,C** show different patterns from **Figure 7A** because the distance measures are essentially defined for point source but with different source locations (i.e., hypocenter versus asperity). The predicted PGA values in **Figures 7B,C** are less than those in **Figure 7A** and are in more agreement with observed ground motion intensity in Kathmandu. **Figure 7D** shows the most significant difference from the observed ground motion intensity in Kathmandu because for all sites above the fault plane, the distance measure is set to R_{jb} = 0.1 km. Indeed, the USGS ShakeMap is similar to **Figure 7D** in terms of amplitude and spatial pattern of the shake map. Importantly, bias in estimated ground motions propagates into rapid earthquake impact assessment. The key issue here is that the current ground motion model together with a finite-fault plane can result in biased predictions of overall earthquake impact (which may affect subsequent decisions for emergency response actions). From practical viewpoints, this issue needs to be resolved in the near future.

[7]http://earthquake.usgs.gov/earthquakes/dyfi/

Earthquake Damage Survey

This section presents main observations and findings from the earthquake damage survey in Nepal. The building typology in Nepal is briefly reviewed, and then, field observations in Kathmandu, Melamchi, Trishuli, and Baluwa are discussed. The regional map of the visited locations is shown in **Figure 3**, and the main survey locations in Kathmandu are indicated in **Figure 4**. The cases discussed in the following are selected to highlight main observations from the survey trip. Numerous photos are available through the Google Earth file as supplementary material to this paper.

Building Typology in Nepal

Buildings in Nepal are vulnerable to seismic actions. The majority of houses and buildings are not seismically designed and constructed, lacking ductile behavior. Due to poor seismic performance, many buildings were damaged/collapsed and these structural failures caused many fatalities during the 2015 earthquake sequences. This subsection briefly summarizes general characteristics of building typology in Nepal. More complete information (e.g., statistics of building characteristics) is available in Chaulagain et al. (2015). According to the 2011 National Population and Housing Census, the total number of individual households in Nepal is 5,423,297, while the population is 26,494,504. The census data indicate that mud-bonded brick/stone masonry buildings are the most common in all geographical regions of Nepal (44.2%), followed by wooden buildings (24.9%). In urban areas (e.g., Kathmandu Valley), buildings with cement-bounded brick/stone (17.6%) and cement concrete (9.9%) are popular.

In Nepal, many masonry buildings are constructed with walls made of sun-dried/fired bricks or stone with mud mortar, and the building frame is made of wood. These types of buildings generally have flexible floors and roof, and are prevalent in rural areas. The masonry materials are of low strength and thus are seismically vulnerable. Recently, with the advancement of the cement in Nepal, brick/stone buildings are constructed with cement mortar. The wooden buildings are popular near the forest areas in Nepal. In these buildings, wooden pillars are made out of tree trunks and walls are constructed with wooden planks or bamboo net cement/mud mortar plaster. The reinforced concrete (RC) building is a modern form of construction in Nepal, which began in late 1970s. The RC moment resisting frame assembly is comprised of cast-in-place concrete beams and columns with cast-in-place concrete slabs for floor and roof. Most of the conventional RC constructions are non-engineered (i.e., not structurally designed) and thus lack sufficient seismic resistance. Engineered RC buildings, which are relatively new, often adopt the Indian standard code with seismic provisions.

Survey Results in Kathmandu

Many historical buildings in the Kathmandu Durbar Square (in front of the Old Royal Palace of the former Kathmandu Kingdom and is a UNESCO World Heritage site) were devastated (area 1 in **Figure 4**). **Figure 8A** shows the collapse of the Basantapur Tower. The complete destruction in the Durbar Square was in sharp contrast with undamaged buildings surrounding the Durbar Square (**Figure 8B**; several wall cracks can be found on these buildings;

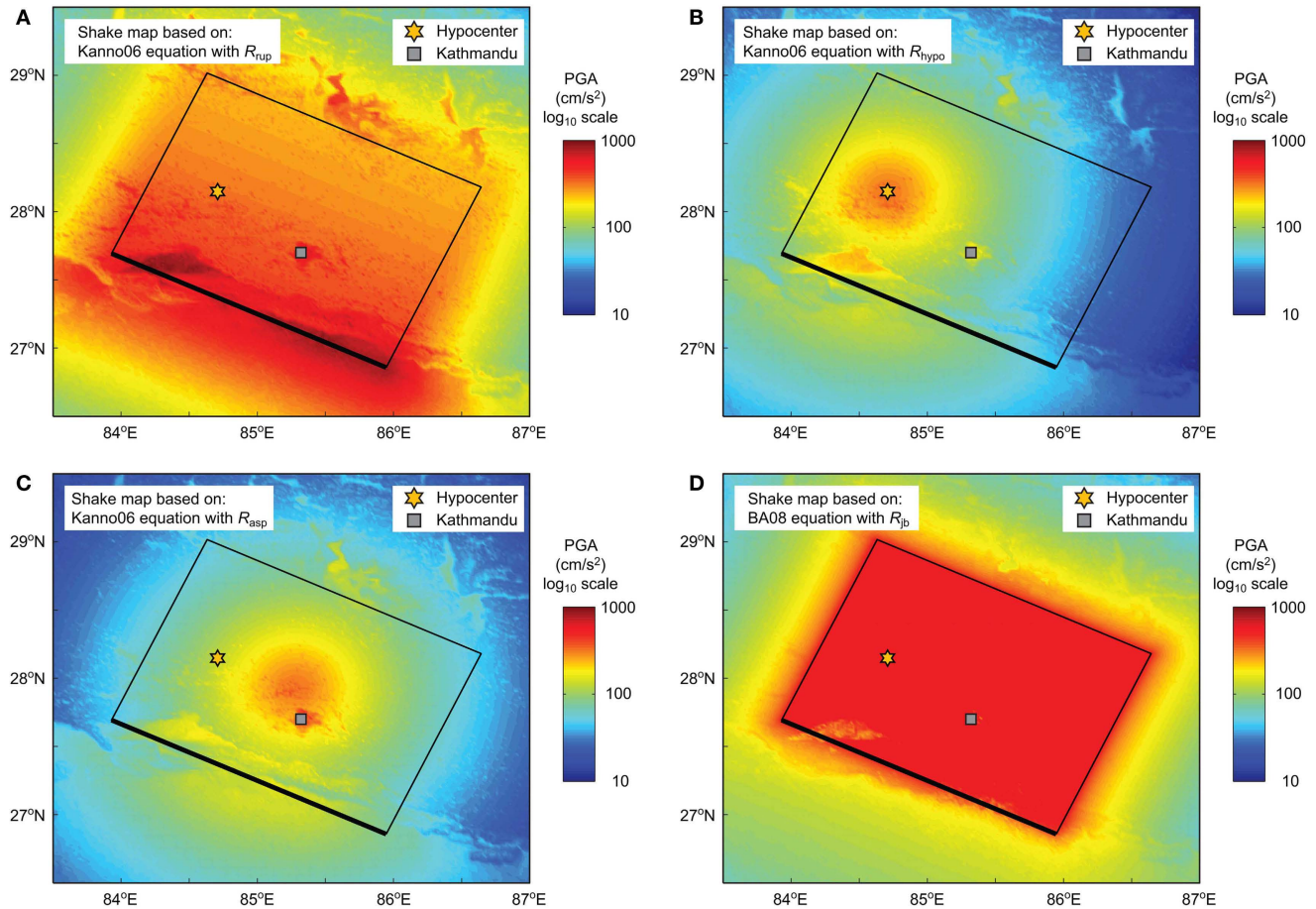

FIGURE 7 | Comparison of scenario shake maps for the M_w7.8 mainshock using: (A) the Kanno06 equation with rupture distance (R_{rup}), (B) the Kanno06 equation with hypocentral distance (R_{hypo}), (C) the Kanno06 equation with distance closest to the asperity (R_{asp}), and (D) the BA08 equation with Joyner–Boore distance (R_{jb}).

however, the majority of the masonry buildings are structurally stable). This indicates that the ground shaking experienced in this area (note: this is relatively close to the KATNP station; see **Figure 4**) was sufficient to cause the collapses of the old historical buildings but was not to cause severe damage to the surrounding buildings. This observation was confirmed by walking through the Indra Chowk area (market squares near the Old Palace), where many old masonry buildings (three to six stories) were densely constructed. Nevertheless, there were several buildings that collapsed completely and some search and rescue activities were undertaken (**Figures 8C,D**).

There were numerous building collapses in the north–west section of the Ring Road along the Bishnumati River (area 2 in **Figure 4**). According to the local geomorphological map, sites within about 300 m from the river are alluvial (Holocene) soil deposits, whereas sites farther east are Pleistocene soil deposits. Therefore, site amplification effects due to different soil conditions may be expected in this area. A walk-through survey was carried out to investigate the spatial distribution of collapsed and severely damaged buildings in this area. Out of 28 collapsed or severely damaged buildings, 19 buildings were in the alluvial deposit area (**Figure 9A**), whereas 9 buildings were in the Pleistocene deposit area but nearer to the boundary (**Figure 9B**). This qualitatively confirms the effects of local site conditions on the building damage and collapse.

In area 3, there was a 16-story high-rise apartment complex (Park View Horizon). The walls of this building suffered from many major cracks along its height (**Figure 9C**). Currently, the apartments are unfit for living and residents have evacuated. The causes of the major damage of the Horizon apartments (and similar high-rise buildings in Kathmandu) may be attributed to the long-period ground motions (**Figure 5**). In addition, local topological features may have contributed to extensive damage there (the complex is on a hill).

Along the Araniko Highway between Kathmandu and Bhaktapur (area 4 in **Figure 4**), a section of the highway (about 200 m in length) built upon embankments was damaged due to the ground settlement. The amount of settlements was about 0.5–2.0 m, depending on locations (**Figure 9D**). The central section of the highway was constructed using reinforced soil retaining wall and

FIGURE 8 | **Damage in Kathmandu (area 1 in Figure 4)**. **(A)** Collapse of the Basantapur Tower in the Kathmandu Durbar Square. **(B)** Undamaged buildings opposite of the Basantapur Tower in the Kathmandu Durbar Square. **(C)** Collapse of four 5- or 6-story old masonry buildings. **(D)** Collapse of a 4-story masonry building.

gravity-type retaining wall (2–3 m high and 100 m wide). The retaining walls were structurally intact and suffered from minor cracks and outward deformation only, whereas the natural slopes at both ends of the highway embankments experienced noticeable settlements (**Figure 9E**). Several buildings along the highway were tilted due to the settlements. A pedestrian footbridge crossing the highway suffered from the differential settlement of foundation, resulting in a gap of 45 cm between the bridge girder and the stair steps.

In area 5 (**Figure 4**), minor liquefaction, which was evidenced by sand boils and did not cause any structural damage, was observed in a small open land near a canal. In the surveyed area, a church was collapsed due to the ground shaking (**Figure 9F**). According to local residents, the church building was standing after the M_w7.8 mainshock but was collapsed due to the M_w6.7 aftershock on the following day. The extent of structural damage before the M_w6.7 aftershock is unknown. There were several houses that settled and tilted in this area. However, the degree of destruction in this area was minor.

Overall, earthquake damage in Kathmandu was not widespread but more localized. This may suggest that overall strong shaking experienced in Kathmandu was not extremely large. The areas that suffered from major destruction tend to have some local characteristics, such as soft soil conditions and structural deficiencies.

Survey Results in Melamchi

The survey was conducted along the road to Melamchi (about 30 km north–east of Kathmandu; **Figure 3**). Melamchi and the surrounding areas were close to the locations of major aftershocks (i.e., 26 April M_w6.7 aftershock and 12 May M_w7.3 aftershock; **Figures 2A** and **3**), and suffered from devastation due to these earthquakes. On the way to Melamchi, there were many small villages that suffered from earthquake damage. During interviews with local residents, they expressed serious concerns about incessant aftershocks and urgent need of repairs of the damaged houses before the arrival of rainy season. Proceeding north toward Melamchi, the occurrence of earthquake damage becomes more frequent.

Melamchi is a small town along the Indrawati River, and residents in the town have been involved with a major Melamchi Water Supply project[8], which diverts the river and channels its water to Kathmandu through tunnels. There were several factories along the road, which make water main pipes. Overall, the earthquake damage in Melamchi was severe, mostly affecting vulnerable masonry buildings, whereas the damage to RC buildings (4- to 5-story) was limited. For instance, the main

[8]http://www.melamchiwater.org/home/

FIGURE 9 | **Damage in Kathmandu (areas 2–5 in Figure 4)**. **(A)** Collapsed building along the Bishnumati River (alluvial soil deposit area; area 2 in **Figure 4**). **(B)** Collapsed building (soft story collapse) near the Bishnumati River (boundary between alluvial and Pleistocene soil deposit areas; area 2 in **Figure 4**). **(C)** Horizon apartment buildings (area 3 in **Figure 4**). **(D)** Settlement of the Araniko Highway (area 4 in **Figure 4**). **(E)** Damage to the Araniko Highway (area 4 in **Figure 4**). **(F)** Collapsed church in the Imadol area (area 5 in **Figure 4**).

street of Melamchi was not completely destroyed (**Figure 10A**); most buildings looked undamaged based on their appearances, although several buildings were collapsed. On the other hand, buildings along a side street were devastated by the earthquakes (**Figures 10B,C**). The majority of the damaged buildings were made of brick and stone. Along the road, several sections of the slope suffered from shallow landsides (**Figure 10D**), their debris blocked the road at one time but was removed. There was a steel truss bridge with RC deck for vehicle crossing; the bridge was not damaged (inspected from backside). It has been reported that further damage occurred in Melamchi due to the 12 May M_w7.3 aftershock. A further damage survey in Melamchi is required to investigate the effects of the aftershock with respect to the incurred damage prior to the aftershock (although it is beyond the scope of this study).

Survey Results in Trishuli

The survey was conducted along the road to Trishuli (about 30 km north–west of Kathmandu; **Figure 3**). One of the purposes of the trip was to investigate the earthquake damage near the Trishuli

FIGURE 10 | Damage in Melamchi (see Figure 3). **(A)** Main street in Melamchi. **(B)** Damaged stone masonry house. **(C)** Devastated street in Melamchi. **(D)** Shallow landslide along the main road.

hydroelectric station. Trishuli was closer to the hypocenter of the M_w7.8 mainshock, and thus severer damage, in comparison with Kathmandu, was expected. Along the way to Trishuli, earthquake damage in Ranipauwa (about 15 km north–west of Kathmandu) appeared relatively minor. Proceeding further north–west, earthquake damage to houses and landslides along the mountain slopes were observed more frequently. The rock fall, as secondary hazard, can be dangerous; a bus was hit by fallen boulder and several people were killed (**Figure 11A**). In Battar (about 25 km north–west of Kathmandu), a large number of brick/stone masonry buildings were collapsed (**Figure 11B**). The building materials of these damaged buildings were of poor quality; for example, two different types of the fragile bricks were used in one of the damaged houses (**Figure 11C**). According to local residents, many buildings were collapsed due to the 25 April M_w6.6 aftershock, which occurred 30 min after the mainshock.

In Trishuli, there was an earth fill dam for hydroelectric power generation. The main body of the dam was the excavated and compacted soil. The height of the dam was 12 m (upstream side) and 20 m (downstream side), and the crest width was about 4 m. Due to the earthquake, there were cracks at upstream side of the dam and fissures on the crest. Moreover, liquefaction (as evidenced by silt boils) and lateral spreading (**Figure 11D**) occurred inside of the dam reservoir due to the earthquake. The operation of the power generation had been suspended since the following day of the mainshock; at the time of the visit, no power was available in nearby villages. Overall, the earthquake damage to the Trishuli dam will not cause severe problems immediately. However, the extent of cracking along the dam axis may suggest a deterioration of the dam body, which may be accelerated into the dam failure by future earthquakes or penetration of rain water into the dam body through cracks. It is important to mention that in worst-case scenarios (note: this earthquake is not the extreme case in terms of ground shaking intensity), catastrophic dam failures could have been caused. As there are several major hydroelectric projects along the Trishuli River as well as in other major rivers in Nepal, ensuring dam safety against large earthquakes is important.

Survey Results in Baluwa

The survey team visited Baluwa (about 70 km north–west of Kathmandu; **Figure 3**) along the Daraudi River, which is close to the epicenter of the M_w7.8 mainshock. One of the aims for this visit was to investigate the earthquake damage very near to the epicenter. Along the Kathmandu–Pokhara highway (e.g., Abu Khaireni, a town located at an intersection between the main highway and the Daraudi link road; about 30 km from the epicenter), no major earthquake damage was observed. At distances of about 18 km from the epicenter, earthquake damage to houses was observed; proceeding further north toward Baluwa, the extent

FIGURE 11 | Damage in Trishuli (see Figure 3). **(A)** Destroyed bus due to boulder fall. **(B)** Damaged brick masonry house in Battar. **(C)** Different types of bricks used in the damaged masonry house in Battar. **(D)** Ground fissures in the Trishuli dam reservoir.

of earthquake damage to houses became severer. The first stone house that was collapsed due to the earthquakes was about 4.5 km from the epicenter. Similarly, many shallow landslides and rock falls were observed along the road to Baluwa (**Figure 12A**); the first middle-size landslide was observed at distances of about 15 km from the epicenter. At one location, the debris from a landslide blocked the road completely (**Figure 12B**; note: detour was possible). The spatial distribution of the collapsed houses and landslides was limited to the locations near the epicenter (within 10–15 km radius), and was in contrast with Melamchi and Trishuli (i.e., farther from the epicenter). This can be understood by referring to the slip distribution of the mainshock (**Figures 2A** and **3**).

A large slope failure was observed at the northern boundary of Baluwa (**Figure 12C**); the length and height of the slope failure were 300 and 100 m, respectively. The fallen boulders and debris blocked the road completely, disconnecting villages at the upstream of the Daraudi River (e.g., Barpak, 5 km north of Baluwa); people can reach these places on foot only. This hampered rescue and recovery activities by governments and international aid teams significantly, highlighting the importance of functional critical infrastructure during the natural disaster emergency. The houses in Baluwa were devastated by the earthquakes and many residents lived in tents (**Figure 12D**). Local residents mentioned that the number of fatalities in Baluwa was small because many of the residents were in the field for agricultural work at the time of the earthquake. Major concerns about the arrival of rainy season were expressed by the local residents.

Conclusion

The M_w7.8 subduction earthquake occurred along the Main Himalayan Thrust arc and triggered numerous major aftershocks. The earthquake damage was catastrophic, causing the fatalities of more than 8,500 and billions of dollars in economic loss. This paper presented important earthquake field observations in Nepal in the aftermath of the M_w7.8 mainshock. A unique aspect of the earthquake damage investigation is that the data were collected 6–11 days after the mainshock, and thus first-hand earthquake damage observations were obtained. To share the gathered damage data widely, geo-tagged photos with observation comments were organized using Google Earth and the kmz file was made publicly available. In the future, the updated version of the Google Earth file, containing more damage photos and measurements from follow-up investigations, will be available from http://www.gdm.iis.u-tokyo.ac.jp/index_e.html. Viewers can download the photos directly and can use them for research and educational purposes. To gain deeper understanding of the observed earthquake damage in Nepal, the seismotectonic setting and regional seismicity in Nepal were reviewed and available aftershock data and ground motion data were analyzed. In addition to ground motion data analysis, scenario shake maps were generated by trialing different combinations of applicable ground motion models and source-to-site distance measures to highlight the potential biases caused in estimated ground motion maps and prompt earthquake impact assessments for a large subduction earthquake.

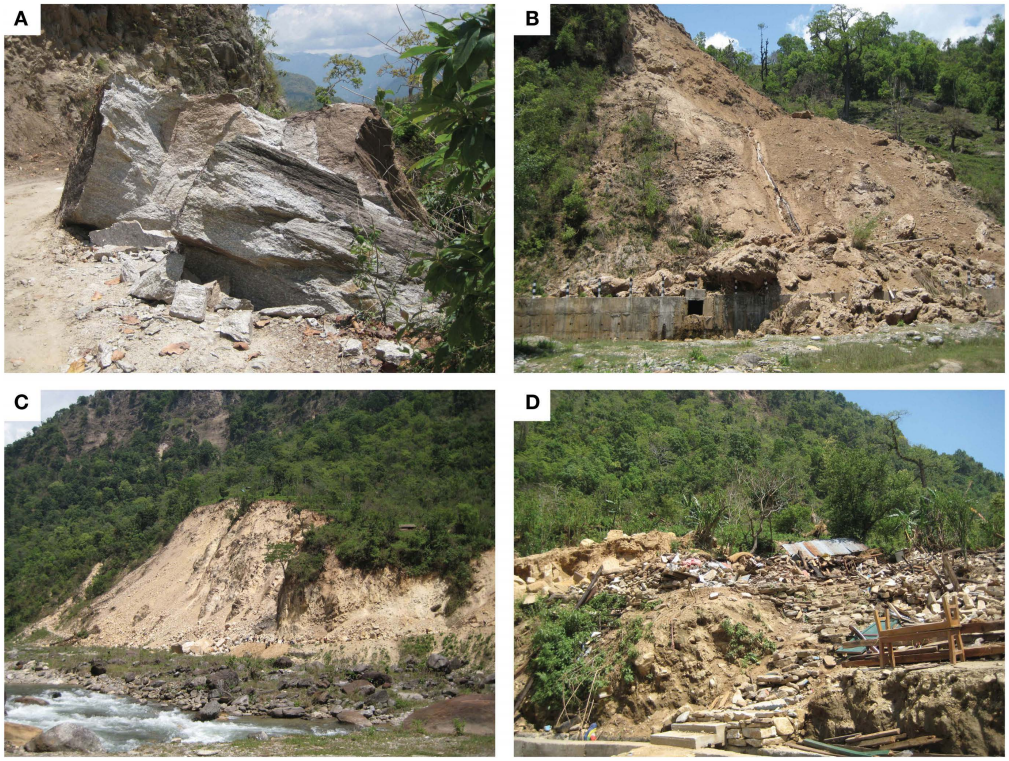

FIGURE 12 | Damage in Baluwa (see Figure 3). **(A)** Fallen boulder. **(B)** Shallow landslide; debris blocked the road. **(C)** Large landslide (100 m high and 300 m wide); debris blocked the road and disconnected villages further north of Baluwa. **(D)** Devastated houses in Baluwa.

The main results from the earthquake damage surveys in Nepal are as follows:

1. In Kathmandu, earthquake damage to old historical buildings was severe, whereas damage to the surrounding buildings was limited. The damaged buildings were stone/brick masonry structures with wooden frames. The RC frame buildings performed well for this earthquake. This may indicate that ground motion intensity experienced in Kathmandu was not so intense, in comparison with those predicted from probabilistic seismic hazard studies for Nepal. Therefore, a caution is necessary related to future earthquakes in Nepal because the 2015 earthquake is not necessarily the worst-case scenario.
2. The Kathmandu Basin is deposited by thick soft sediments. This has led to the generation of long-period ground motions in the Kathmandu Valley. Although the majority of the existing buildings in Kathmandu were not directly affected by the long-period ground motions, such seismic waves can pose serious risks to high-rise buildings. Adequate earthquake engineering design considerations are essential for reducing potential seismic risk to these structures.
3. The building damage in Kathmandu was localized to specific areas. It appeared that the building collapse sites were affected by local soil characteristics and/or structural deficiencies. In this regard, microzonation studies provide valuable insights into earthquake damage occurrence.
4. Some buildings that were severely damaged by the mainshock were collapsed due to major aftershocks. The capability for aftershock forecasting, building evacuation procedure, building inspection and tagging, and building repairs and retrofitting (low-cost solutions) need to be improved to mitigate the earthquake damage potential.
5. In the mountain areas, numerous villages were devastated by the earthquake sequence and major landslides were triggered. On occasion, landslides blocked roads, disconnecting remote villages. The redundancy of the local transportation network in Nepal needs to be improved for enhancing the resilience of rural communities.

Acknowledgments

The authors thank Pradeep Pokhrel for his great assistance during the field survey. The financial support by the JSPS KAKENHI (15H02631) is greatly acknowledged. The work was also funded by the EPSRC grant (EP/I01778X/1) for the Earthquake Engineering Field Investigation Team (EEFIT).

Supplementary Material

The Supplementary Material for this article can be found online at http://journal.frontiersin.org/article/10.3389/fbuil.2015.00008

References

Ader, T., Avouac, J. P., Liu-Zeng, J., Lyon-Caen, H., Bollinger, L., Galetzka, J., et al. (2012). Convergence rate across the Nepal Himalaya and interseismic coupling on the Main Himalayan fault: implications for seismic hazard. *J. Geophys. Res.* 117, B04403. doi:10.1029/2011JB009071

Ambraseys, N. N., and Douglas, J. (2004). Magnitude calibration of north Indian earthquakes. *Geophys. J. Int.* 159, 165–206. doi:10.1111/j.1365-246X.2004.02323.x

Atkinson, G. M., and Wald, D. J. (2007). Did you feel it? intensity data: a surprisingly good measure of earthquake ground motion. *Seismol. Res. Lett.* 78, 362–368. doi:10.1785/gssrl.78.3.362

Avouac, J. P. (2003). Mountain building, erosion and the seismic cycle in the Nepal Himalaya. *Adv. Geophys.* 46, 1–80. doi:10.1016/S0065-2687(03)46001-9

Bilham, R. (2004). Earthquakes in India and the Himalaya: tectonics, geodesy and history. *Ann. Geophys.* 47, 839–858. doi:10.4401/ag-3338

Boore, D. M., and Atkinson, G. M. (2008). Ground motion prediction equations for the average horizontal component of PGA, PGV, and 5% damped PSA at spectral periods between 0.01 s and 10.0 s. *Earthquake Spectra* 24, 99–138. doi:10.1193/1.2830434

Boore, D. M., Stewart, J. P., Seyhan, E., and Atkinson, G. M. (2014). NGA-West2 equations for predicting PGA, PGV, and 5% damped PSA for shallow crustal earthquakes. *Earthquake Spectra* 30, 1057–1085. doi:10.1193/070113EQS184M

Center for Disaster Management and Risk Reduction Technology (CEDIM). (2015). *Nepal Earthquakes – Report #3*. Available at: https://www.cedim.de/english/index.php

Chaulagain, H., Rodrigues, H., Spacone, E., and Varum, H. (2015). Seismic response of current RC buildings in Kathmandu Valley. *Struct. Eng. Mech.* 53, 791–818. doi:10.12989/sem.2015.53.4.791

Goda, K., and Atkinson, G. M. (2014). Variation of source-to-site distance for megathrust subduction earthquakes: effects on ground motion prediction equations. *Earthquake Spectra* 30, 845–866. doi:10.1193/080512EQS254M

Gupta, I. D. (2006). Delineation of probable seismic sources in India and neighbourhood by a comparative analysis of seismotectonic characteristics of the region. *Soil Dynam. Earthquake Eng.* 26, 766–790. doi:10.1016/j.soildyn.2005.12.007

Harbindu, A., Gupta, S., and Sharma, M. L. (2014). Earthquake ground motion predictive equations for Garhwal Himalaya, India. *Soil Dynam. Earthquake Eng.* 66, 135–148. doi:10.1016/j.soildyn.2014.06.018

Heuret, A., Lallemand, S., Funiciello, F., Piromallo, C., and Faccenna, C. (2011). Physical characteristics of subduction interface type seismogenic zones revisited. *Geochem. Geophys. Geosyst.* 12, Q01004. doi:10.1029/2010GC003230

Hong, H. P., and Goda, K. (2007). Orientation-dependent ground-motion measure for seismic-hazard assessment. *Bull. Seismol. Soc. Am.* 97, 1525–1538. doi:10.1785/0120060194

Huang, Y. N., Whittaker, A. S., and Luco, N. (2008). Maximum spectral demands in the near-fault region. *Earthquake Spectra* 24, 319–341. doi:10.1193/1.2830435

Jaiswal, K. S., and Wald, D. J. (2010). An empirical model for global earthquake fatality estimation. *Earthquake Spectra* 26, 1017–1037. doi:10.1193/1.3480331

Ji, C. (2008). *Preliminary Result of the May 12, 2008 M_w 7.97 Sichuan Earthquake*. Available at: http://www.geol.ucsb.edu/faculty/ji/big_earthquakes/2008/05/12/ShiChuan.html

Kanno, T., Narita, A., Morikawa, N., Fujiwara, H., and Fukushima, Y. (2006). A new attenuation relation for strong ground motion in Japan based on recorded data. *Bull. Seismol. Soc. Am.* 96, 879–897. doi:10.1785/0120050138

Lu, M., Li, X. J., An, X. W., and Zhao, J. X. (2010). A comparison of recorded response spectra from the 2008 Wenchuan, China, earthquake with modern ground-motion prediction models. *Bull. Seismol. Soc. Am.* 100, 2357–2380. doi:10.1785/0120090303

Mai, P. M., Spudich, P., and Boatwright, J. (2005). Hypocenter locations in finite-source rupture models. *Bull. Seismol. Soc. Am.* 95, 965–980. doi:10.1785/0120040111

Nath, S. K., and Thingbaijam, K. K. S. (2011). Peak ground motion predictions in India: an appraisal for rock sites. *J. Seismol.* 15, 295–315. doi:10.1007/s10950-010-9224-5

Nath, S. K., and Thingbaijam, K. K. S. (2012). Probabilistic seismic hazard assessment of India. *Seismol. Res. Lett.* 83, 135–149. doi:10.1785/gssrl.83.1.135

Paudyal, Y. R., Bhandary, N. P., and Yatabe, R. (2012). Seismic microzonation of densely populated area of Kathmandu Valley of Nepal using microtremor observations. *J. Earthquake Eng.* 16, 1208–1229. doi:10.1080/13632469.2012.693242

Ram, T. D., and Wang, G. (2013). Probabilistic seismic hazard analysis in Nepal. *Earthquake Eng. Eng. Vib.* 12, 577–586. doi:10.1007/s11803-013-0191-z

Sakai, H., Fujii, R., and Kuwahara, Y. (2002). Changes in the depositional system of the Paleo-Kathmandu Lake caused by uplift of the Nepal Lesser Himalayas. *J. Asian Earth Sci.* 20, 267–276. doi:10.1016/S1367-9120(01)00046-3

Sharma, M. L., Douglas, J., Bungum, H., and Kotadia, J. (2009). Ground-motion prediction equations based on data from Himalayan and Zagros regions. *J. Earthquake Eng.* 13, 1191–1210. doi:10.1080/13632460902859151

Shcherbakov, R., Goda, K., Ivanian, A., and Atkinson, G. M. (2013). Aftershock statistics of major subduction earthquakes. *Bull. Seismol. Soc. Am.* 103, 3222–3234. doi:10.1785/0120120337

Shcherbakov, R., Turcotte, D. L., and Rundle, J. B. (2005). Aftershock statistics. *Pure Appl. Geophys.* 162, 1051–1076. doi:10.1007/s00024-004-2661-8

Stern, R. J. (2002). Subduction zones. *Rev. Geophys.* 40, 1012. doi:10.1029/2001RG000108

Takewaki, I., Murakami, S., Fujita, K., Yoshitomi, S., and Tsuji, M. (2011). The 2011 off the Pacific coast of Tohoku earthquake and response of high-rise buildings under long-period ground motions. *Soil Dynam. Earthquake Eng.* 31, 1511–1528. doi:10.1016/j.soildyn.2011.06.001

United Nations Office for the Coordination of Humanitarian Affairs (UN-OCHA). (2015). Available at: http://www.unocha.org/nepal

United States Geological Survey (USGS). (2015). Available at: http://earthquake.usgs.gov/earthquakes/eventpage/us20002926#scientific_finitefault

Wald, D. J., and Allen, T. I. (2007). Topographic slope as a proxy for seismic site conditions and amplification. *Bull. Seismol. Soc. Am.* 97, 1379–1395. doi:10.1785/0120060267

Wald, D. J., Worden, B. C., Quitoriano, V., and Pankow, K. L. (2005). *ShakeMap Manual: Technical Manual, User's Guide, and Software Guide*. Golden, CO: U.S. Geological Survey, 132.

Yagi, T. (2015). Available at: http://www.geol.tsukuba.ac.jp/~yagi-y/EQ/20150425/index.html

Conflict of Interest Statement: The authors declare that the research was conducted in the absence of any commercial or financial relationships that could be construed as a potential conflict of interest.